Ultrasonically-enhanced convective heat transfer: Evidence of a relationship with the thermal boundary layer

Christophe Poncet, Sébastien Ferrouillat, Laure Vignal, Antoine Courouble, Odin Bulliard-Sauret, Nicolas Gondrexon

Ultrasonically-enhanced convective heat transfer: Evidence of a relationship with the thermal boundary layer

Christophe Poncet[1], Sébastien Ferrouillat[1], Laure Vignal[1], Antoine Courouble[1], Odin Bulliard-Sauret[1], and Nicolas Gondrexon[2]

[1]Université Grenoble-Alpes, CNRS, Grenoble INP, LEGI, 38000 Grenoble, France
[2]Université Grenoble-Alpes, CNRS, Grenoble INP, LRP, 38000 Grenoble, France

Nomenclature

Latin symbols

d	Channel width	m
D_h	Hydraulic diameter	m
e	Distance between 2 points	m
h	Heat transfer coefficient	$W.m^{-2}.K^{-1}$
HTEF	Heat Transfer Enhancement Factor	%
k	Thermal conductivity	$W.m^{-1}.K^{-1}$
L_c	Characteristic length	m
L_e	Hydrodynamic entrance length	m
Nu	Nusselt number	-
Re	Reynolds number	-
S	Heat exchange surface	m^2
T	Temperature	°C
TKE	Turbulent Kinetic Energy	$m^2.s^{-2}$
U	Velocity	$m.s^{-1}$

Greek symbols

δ	Boundary layer thickness	m
Φ	Thermal power	W

Subscripts

avg	Average
fluid	related to the fluid
inst	Instantaneous
lam	Laminar regime

silent	Without ultrasound
th	Thermal
turb	Turbulent regime
us	In presence of ultrasound
w	Related to the heating wall

Abstract

The influence of ultrasound on convective heat transfer depending on the flow regime is investigated in this study, using an experimental setup consisting of a rectangular channel with a heating plate on one side and an ultrasonic transducer opposite it on the other. In order to understand the physical phenomena taking place, this work was based on two approaches. The first one focuses on hydrodynamic analysis using Particle Image Velocimetry, focusing specifically on the influence of ultrasound on velocity fields. The second approach aims to determine the convective heat transfer coefficient and Nusselt number, by measuring fluid and heating plate temperatures. Experimental results show that 25 kHz ultrasound allows heat transfer to be enhanced over the Reynolds number range studied, from a laminar regime (Re=890) to a turbulent regime (Re=14500), as the acoustic cavitation induce disturbances within the thermal boundary layer. The heat transfer enhancement factor decreases as the Reynolds number increases, until an asymptote is reached in the turbulent regime. For 2 MHz ultrasound, the acoustic streaming generated allows to improve convective effects within the flow, consequently enhancing heat transfer. The heat transfer enhancement factor decreases as the Reynolds number increases up to 7500, at which point 2 MHz ultrasound no longer induces heat transfer enhancement. Finally, ultrasonically induced heat transfer enhancement has been analyzed in terms of the initial thermal boundary layer thickness for silent conditions. The overall results of this study demonstrate the existence of a strong relationship between heat transfer enhancement and initial thermal boundary layer thickness. The thicker the silent initial thermal boundary layer, the greater the heat transfer enhancement.

1 Introduction

1.1 Bibliographic survey

Many industrial processes involve heat transfer from one fluid to another. From an energy optimization perspective, the design and development of more efficient heat exchangers is of great interest. For this purpose, a wide variety of heat transfer enhancement techniques has been explored. For single phase heat transfer, enhancement methods are usually classified either as passive, which are generally based on surface and design modifications to increase fluid turbulence, or as active, requiring external source of energy to purposely induce turbulence, and thus enhance heat transfer [1]. Among the existing active methods, the use of ultrasound has repeatedly been shown to enhance convective heat transfer in natural convection, but also in forced convection, especially in a configuration representative of a heat exchanger, even though this has been studied to a lesser extent than in natural convection.

Ultrasound is an acoustic wave with a frequency ranging between 20 kHz and 10 MHz. The 20 kHz and 100 kHz range is generally defined as low-frequency. Above 100 kHz, ultrasound is categorized as high-frequency. Another distinction generally used to characterize ultrasound is ultrasonic power, which leads to different applications, widely detailed by Yao *et al.* (2020) [2].

When ultrasonic waves propagate in a liquid medium, they induce two main hydrodynamic phenomena. The first one is acoustic cavitation, which is the process of formation, expansion, oscillation and implosion of bubbles of vapor and gases that were originally dissolved in a liquid medium. Acoustic cavitation is induced by the pressure variation generated by an acoustic wave reaching a threshold, in which vapor pressure, tensile strength, and the quantity of dissolved gases play an important role. The intensity of acoustic cavitation depends on several parameters related to fluid properties, such as surface tension and viscosity [3]. Cavitational intensity is also related to ultrasound parameters, such as acoustic power, with higher acoustic power inducing greater cavitational intensity. Moreover, the acoustic cavitation threshold strongly depends on frequency, with low frequencies

tending to facilitate generation of cavitation bubbles [4]. Finally, the resonance size of a bubble is inversely related to the applied frequency, thus low-frequency acoustic fields produce mostly larger bubbles than high-frequency acoustic fields. Cavitation produces strong hydrodynamic effects within liquid. During the expansion and compression phases, the oscillations of the cavitation bubbles may produce convective flows at the scale of the bubble. In addition, implosion of the bubbles generates large shock waves within the liquid, which can then cause nearby bubbles to implode. Finally, the implosion of asymmetric bubbles also generates a micro-jet of fluid at very high speed [5]. Therefore, hydrodynamic effects generated by acoustic cavitation are mostly located around bubbles, at the micro-scale.

On the other hand, when ultrasound is generated within liquids, the acoustic energy carried by the wave is dissipated within the medium. The wave attenuation induces a pressure gradient within the liquid and thus produces recirculation flows (zero net mass flow) in the same direction as the acoustic field. These flows are known as Eckart streaming. Acoustic attenuation is usually stronger with high frequencies resulting in stronger Eckart streaming in the presence of high ultrasonic frequencies. Nevertheless, high acoustic power density leads to high bubble density resulting in strong acoustic impedance that opposes acoustic wave propagation. This acoustic wave attenuation due to the presence of bubbles may also induce acoustic streaming, as shown by Nomura et al. (2002) [6], for example. Acoustic streaming thus occurs at a macroscopic scale within the liquid.

Several studies have shown that ultrasound can disturb the hydrodynamics of a liquid flow, and increases its turbulent intensity. These perturbations strongly depend on the effects generated by ultrasound. Acoustic cavitation, which generates mostly local effects, seems to induce some localized velocity fluctuations [7], leading to turbulence production within the liquid flow, as suggested by several authors [8–10]. Acoustic cavitation ensures that parietal transfers increase, and that boundary layer thickness can be reduced, even when convective effects induced by acoustic cavitation seem to have fully dissipated [11]. Moreover, some studies suggest that in the presence of acoustic cavitation, the fluid velocity can induce an increase in the intensity of acoustic cavitation, due to the reduced coalescence of bubbles [12]. On the other hand, when acoustic streaming is generated perpendicular to the flow, the fluid flow is driven away from the transducer. In addition, the increase in flow velocity induces an attenuation of the transverse velocities initially generated by acoustic streaming [11]. It has also been shown that Eckart-type acoustic streaming produced by high frequency ultrasound tends to generate turbulent kinetic energy within the fluid flow. However, this ultrasonically-induced kinetic energy is highly sensitive to liquid flow, causing it to decrease as the liquid flow rate and velocity increase [13].

Based on all these studies, the hydrodynamic effects produced by ultrasound when ultrasonic fields are generated in a liquid flow can be identified. It is then possible to analyze the changes in these effects as a function of the flow regime. Indeed, ultrasound allows the momentum transfer to be increased when the flow regime is laminar, and also leads to instantaneous velocity fluctuations. In turbulent flow, these effects can be considerably lower, depending on the ultrasonic frequency and the power used.

Consideration of these strong hydrodynamic effects generated by ultrasound provides some basis for an explanation of how ultrasound can enhance heat transfer. By generating disturbances within the fluid, ultrasound may thus reduce the thermal boundary layer and consequently enhance heat transfer. Several works have studied natural convection enhanced by ultrasound [14–16]. Some authors looked at low-frequency ultrasound, and their results showed that when acoustic cavitation was generated close to a heating surface, the heat transfer coefficient improved [17, 18]. The authors suggested that acoustic cavitation may disturb the thermal boundary layer, thus resulting in heat transfer enhancement. Some studies have also shown that acoustic streaming, when generated close to a heating surface, may disturb the thermal boundary layer and thus improve convective heat transfer [6, 19].

However, the influence of ultrasound on heat transfer in forced convection has been

studied to a considerably lesser extent until now. Several studies have been carried out on heat exchangers using ultrasound to enhance heat transfer and have led to some conclusions on the interaction between ultrasound and heat transfer in forced convection. Whether with shell and tube heat exchangers [20], or double-pipe heat exchangers [21, 22], studies have shown that ultrasound induces heat transfer enhancement. Nevertheless, increasing the cold water flow rate (*i.e.*, the fluid flow where ultrasound is generated) induces an asymptotic decrease in the heat transfer enhancement. To improve understanding of these tendencies, some research has been conducted into the influence of ultrasound on convective heat transfer in forced convection at a smaller scale.

Inworn *et al.* (2018) [23] studied heat transfer enhancement with low-frequency ultrasound (25 kHz, 33 kHz and 40 kHz) along a hot plate, within a channel with a rectangular cross-section, for different flow velocities. Their results showed that the incidence zone of the ultrasonic field, and thus the zone where heat transfer is intensified, tend to move further downstream as the flow velocity increases, which correlates the results of Barthès *et al.* (2015).

Moreover, as mentioned previously, different physical phenomena induced by acoustic waves may occur (cavitation and acoustic streaming) and interact differently with the fluid flow. Bulliard-Sauret *et al.* (2019) [10] analyzed the influence on heat transfer enhancement induced by low frequency ultrasound (f=25 kHz), which mainly produces acoustic cavitation, compared to high frequency ultrasound (f=2 MHz), which mainly produces acoustic streaming. This study showed that the turbulence generated by low-frequency ultrasound tended to be enhanced with increasing flow velocity in the laminar regime, thus improving the heat transfer enhancement. However, in the case of high frequency ultrasound, the turbulence as well as the heat transfer enhancement generated by the ultrasound tend to attenuate as the flow velocity increases.

1.2 Objectives of this work

Despite all the studies performed on heat transfer enhancement in forced convection in the presence of ultrasound, very little study has been done of certain aspects, such as the effect of variation in the flow regime or ultrasonic frequency on heat transfer enhancement. Moreover, no study on heat transfer enhancement in the presence of ultrasound has been conducted in relation to the thermal boundary layer. Therefore, this work aims to analyze convective heat transfer in forced convection, in the presence of ultrasound, depending on the hydrodynamic conditions of the liquid flow. In addition, the influence of acoustic cavitation and acoustic streaming will be compared and discussed.

For this purpose, an experimental test section was designed, composed of a heating plate and suitable for addition of an ultrasonic transducer. The experimental setup has been designed to ensure controlled hydrodynamic conditions within the test section.

To compare the influence of both acoustic cavitation and acoustic streaming separately, two ultrasonic transducers with different frequencies are used, a 25 kHz transducer which mostly generates acoustic cavitation and a 2 MHz transducer which mostly induces acoustic streaming.

In this study, two different metrological approaches are implemented in parallel. First, a hydrodynamic approach is taken, based on Particle Image Velocimetry (PIV) measurements, to analyze the effects induced by ultrasound on the liquid flow. Secondly, a thermal approach is followed, with temperature measurements taken on a heating plate, allowing the convective heat transfer to be evaluated. The combination of these two approaches provides a more complete understanding of the changes in the fluid flow hydrodynamics and the convective heat transfer, in the presence of ultrasound.

Lastly, the heat transfer enhancement generated by ultrasound is investigated in regard to the initial thermal boundary layer thickness as determined under silent conditions, offering an innovative approach for this enhancement method.

This paper presents the experimental setup implemented for this work, as well as the

analysis methods developed, in order to study the variation in hydrodynamics and heat transfer in the presence of ultrasound. The results obtained are then presented in two parts. The first part is related to changes in hydrodynamics and heat transfer enhancement depending on the flow regime. The second part focuses on analysis of the heat transfer enhancement depending on the thermal boundary layer thickness.

2 Materials and methods

2.1 Experimental setup

The experimental setup is composed of a hydraulic circuit which allows water flow and water temperature to be regulated. The water flows through a test section, where thermo-hydraulic measurements are taken.

The initial test section, designed to study heat transfer enhancement in the presence of ultrasound, was introduced in previous work [13]. In order to provide a fluid flowing vertically and unidirectionally along the heating plate, an inlet and an outlet channel have been designed specifically for this purpose. These two channels are attached respectively at the bottom and the top of the test section, as shown in figure 1 in a light blue color.

The test section is a stainless steel tank (in light gray on figure 1), composed of a heating plate integrated into a mobile structure. Opposite the heating plate, an ultrasonic transducer can be fixed to the tank. The space between the transducer and the heating plate facing it forms a rectangular channel where the fluid flows.

The mobile structure is made of PTFE and provides mechanical support for the heating plate, in addition to thermal insulation, so that heat is assumed to be transmitted towards the fluid flow only. The mobile structure can be moved along the x-axis, thus modifying the channel width d, as represented on figure 2.

An inlet cone is attached to the bottom of the inlet channel, incorporating a porous structure to avoid an inlet jet effect. A honeycomb structure is also placed in the inlet channel just after the porous structure to reduce any vorticity that may be present at the inlet. The distance between the channel inlet and the beginning of the heating plate is 900 mm, and the internal cross-section is 100×100 mm^2. The channel inlet is designed so that a baffle of variable size can be inserted to change the channel width d. The water flow through the test section is represented by the blue arrows in figure 1.

As mentioned in the above, the water flow rate, ranging between 0 to 12.6 L.s^{-1}, can be controlled and measured thanks to the hydraulic circuit, using a regulator valve and a Krohne Waterflux 3100 W flowmeter, with an an uncertainty of 0,3% of the measured value, according to the supplier. An Iwaki MX 251 CV5-E pump is used to make water flow around the circuit. The water temperature at the inlet of the test section is regulated at 20 °C ± 0.5 °C, using an external plate heat exchanger with temperature-controlled water from an external cooling system.

Within the test section, the fluid temperature (T_{fluid}) is measured at the test section inlet, as shown on figure 1. In this work, the fluid temperature difference between the inlet and the outlet is considered negligible, due to the high flow rate in comparison with the thermal power exchanged.

A cross-sectional detail view of the test section is shown in figure 1.

The heating plate is divided into five heating blocks of 19 mm (y-axis) × 18 mm (x-axis) × 90 mm (z-axis) made of 316L stainless steel with a thermal conductivity of k_{316L}=15 W.m^{-1}.K^{-1}. Each stainless steel block is attached to a copper block (in red in figure 2) in which an electric heating rod is placed to impose a thermal flux. The heating blocks are separated from each other by a 1 mm-thick ceramic thermal insulation called Macor®, with a thermal conductivity of k_{Macor} = 1.46 W.m^{-1}.K^{-1}. Finally, the heating plate is insulated with PTFE, as mentioned previously (k_{PTFE}=0.25 W.m^{-1}.K^{-1}). This thermal insulation ensures a unidirectional heat flux through each block, in the negative

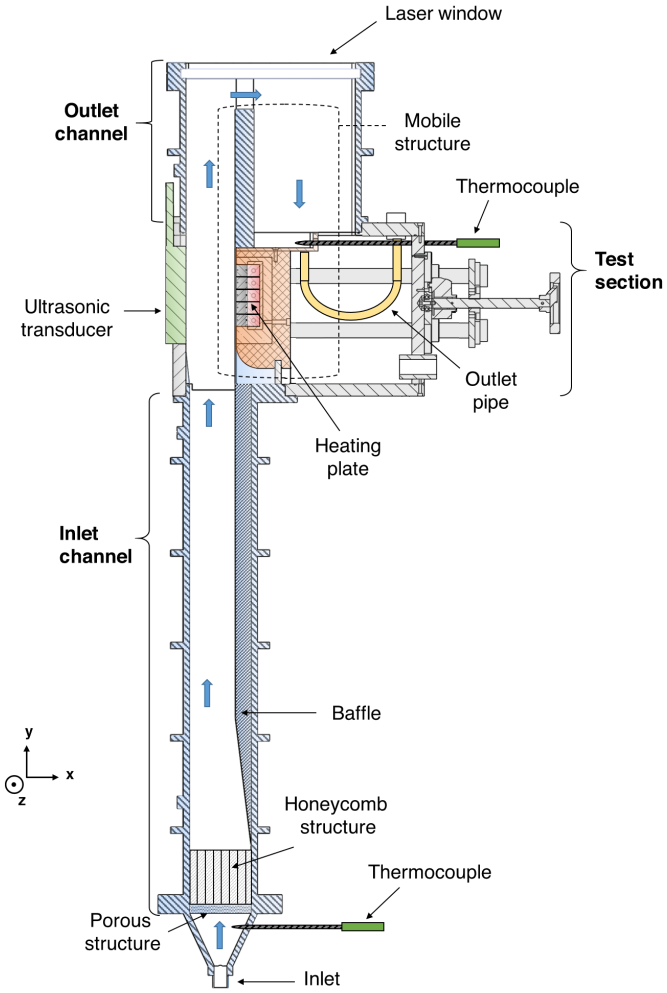

Figure 1 – Cross-sectional view of the test section, inlet channel and outlet channel.

x-direction. The total power supplied to the heating wall (denoted Φ) is equal to 450 W and is assumed to be equally distributed across the 5 heating blocks.

Each block is associated with two thermocouples within the stainless steel blocks, one is located on the wall side (T_1), at 16 mm, from the water/plate interface, the other one is located on the channel side (T_2), at 2 mm from the water/plate interface, as depicted in the insert in figure 2. This thermocouples allows to measure the temperature at different locations on the plate, and then quantify the heat transfer coefficient at the surface of each block, as detailed in part 2.3. The temperature measurements are taken in the stainless steel blocks and not in the copper blocks, to ensure a greater temperature difference between T_1 and T_2 due to the lower thermal conductivity of stainless steel compared to that of copper. The thermocouples are calibrated and have an absolute uncertainty of 0,6°C.

Regarding the test section, as previously stated, the channel width d can be modified, meaning that the heat transfer enhancement generated by ultrasound can be analyzed as a function of the distance between the ultrasonic transducer and the heating plate. In the first part of this paper, the analysis is carried out with a constant channel width of $d = 33\ mm$, corresponding to a hydrodynamically-developed internal flow. In the second part of this article, thermal measurements are also performed with two additional different channel widths, respectively $d = 63\ mm$ and $d = 107.5\ mm$. These two channel widths do not allow hydrodynamic development of the flow within the test section, considering that the hydrodynamic entrance length is greater than the inlet channel. The flow is thus comparable to an external flow. By comparing the results obtained for each of the channel widths, analysis can be made of the phenomenon of heat transfer enhancement by

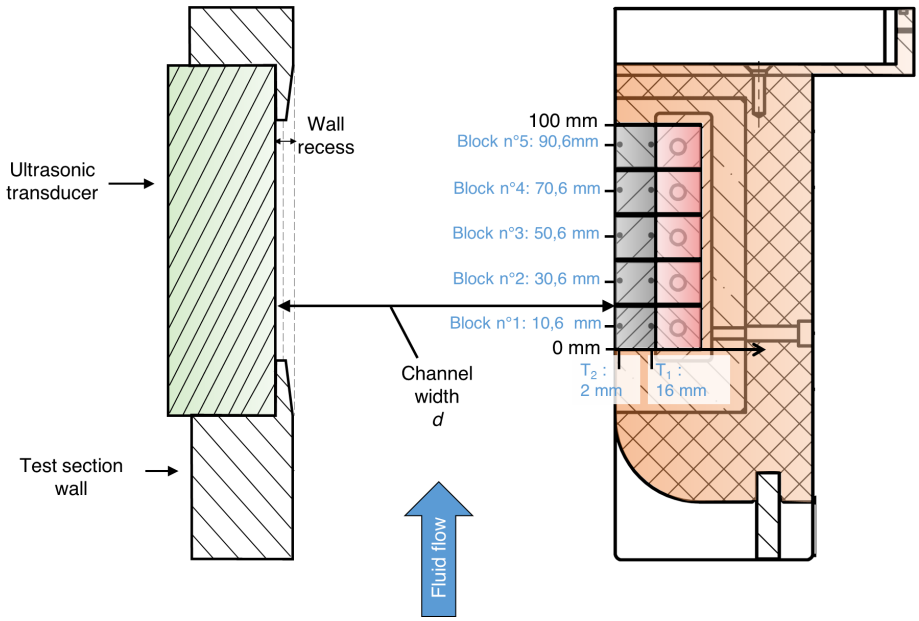

Figure 2 – Detailed cross-sectional view of the test section.

ultrasound, regardless of the type of forced convection used (internal or external).

Finally, regarding the ultrasonic emitters, 2 transducers with different frequencies have been used: a 25 kHz transducer, provided by the Sinaptec® company, and a 2 MHz transducer, which is a commercial product of the Sonosys® company. Their characterization has already been presented in previous work [24]. The 25 kHz transducer mostly generates acoustic cavitation. Qualitative mechanical characterization with aluminum foil has been performed, showing strong erosion induced by acoustic cavitation. On the other hand, the 2 MHz transducer characterization with aluminum foil test has shown no mechanical effect induced by ultrasound at this frequency. Regarding ultrasonic power, the transducers have been characterized using the calorimetric method [25] to ensure that each transducer provides the same power. The ultrasonic power was then set at 110 W for both ultrasonic transducers.

2.2 Hydrodynamic approach

In order to understand the effects of ultrasound within fluid flow, the Particle Image Velocimetry (PIV) technique has been used in several studies [10, 26, 27] and has produced interesting results. PIV is an optical method based on the tracking of groups of particles trajectory of in order to measure the instantaneous velocity field in a flow. In this technique, the fluid is seeded with reflective or fluorescent particles which have a similar density to the fluid and are therefore able to follow the dynamics of the flow as closely as possible. These particles are illuminated by a laser sheet, and the movement of the particles is recorded by a camera placed perpendicular to the direction of incidence of the laser sheet. The time interval dt between each recorded image is determined beforehand. Thus, by measuring the displacement of the particles between two images, the speed of these particles, and subsequently the instantaneous velocity field can be determined. The PIV setup is represented on figure 3.

Here, a two-dimensional two-component (2D-2C) device has been used. The laser is a Nd-Yag (provided by Dantec Dynamics) with two cavities, generating 200 mJ. The camera is an ImagerProX2M (provided by LaVision), with a 1600x1200-pixel resolution. The measuring field of the camera is 140 mm (x-axis) by 100 mm (y-axis), with an effective measuring field of 30 mm (x-axis) by 100 mm (y-axis) which is suitable for analyzing the fluid flow between the heating blocks and the ultrasonic transducer. The recording is carried out in double-frame, meaning that a pair of frames is shot with a given dt between

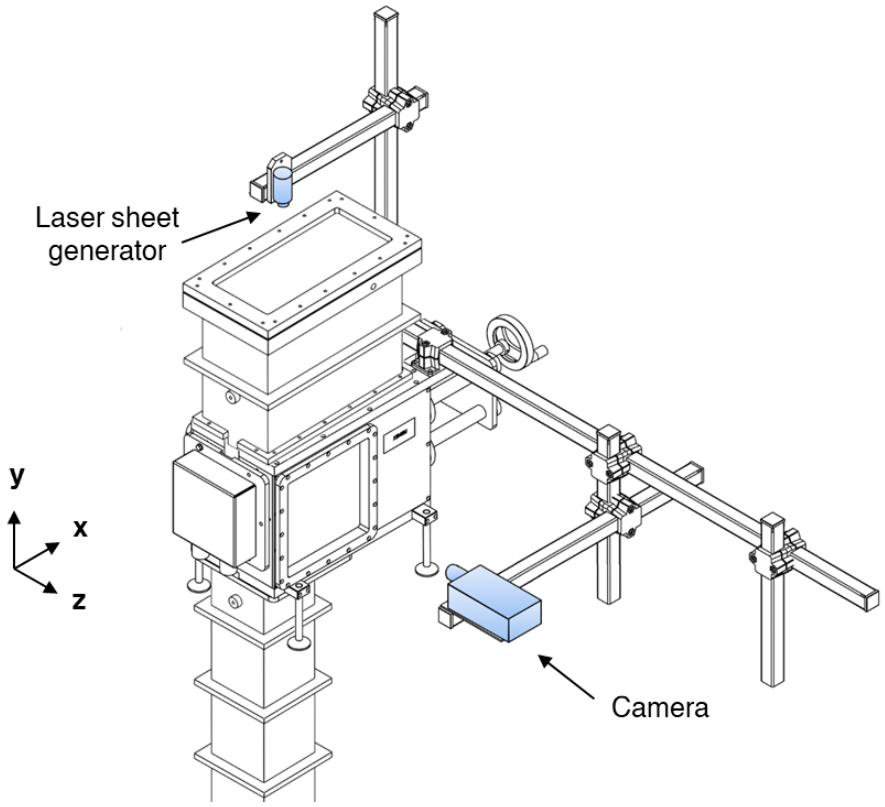

Figure 3 – PIV setup.

two frames. The *dt* is adjusted for an average particle displacement of 8 pixels between 2 frames. Data processing and post-processing are then carried out using Davis 8.3 software (provided by LaVision). The processing calculates the instantaneous velocity field from each pair of frames. The frames are therefore divided into interrogation windows in order to determine the most probable displacement of the particles within the interrogation window. In this work, the displacement vectors are determined by an iterative multi-pass calculation. The first pass is performed with an interrogation window of 32×32 pixels, and the windows overlap by 50%. The final pass is performed with an interrogation window of 16×16 pixels, with no overlap of interrogation windows. The choice of interrogation window sizes was made to ensure that the interrogation windows of the first pass are 4 times larger than the mean displacement (*i.e.*, 8 pixels here), and that the interrogation windows of the last pass retain a sufficient number of particles (*i.e.*, approximately 15 particles per interrogation window).

Once the instantaneous velocity calculations have been completed, post-processing is carried out to eliminate the vectors which have a low correlation value (described in the Davis 8.3 Software product manual [28]) and which therefore induce some uncertainty in the results. In this study, the choice was made to set a minimum correlation value of 0.2. When the correlation value of a displacement vector is lower than this value, the vector is deleted and replaced by a velocity vector resulting from an interpolation of the 8 spatially closest velocity vectors.

For each test, data acquisition results in 2500 instantaneous velocity fields. These instantaneous velocity fields can then be averaged to obtain the average velocity field for the test. It is also possible to calculate the Turbulent Kinetic Energy (TKE), which quantifies the velocity fluctuations resulting from the turbulence present in the flow. In this work, the TKE is used in particular to evaluate the additional turbulence generated by ultrasound. The Turbulent Kinetic Energy is calculated as follows [28]:

$$TKE = \frac{3}{4} \times \sqrt{\frac{\sum_{i=1}^{N}(U_{inst} - U_{avg})^2}{N-1}}^2 \quad (1)$$

PIV measurements have been carried out first without ultrasound, in laminar and turbulent regimes. To assess the effect of ultrasound on velocity fields and turbulence within the fluid flow, measurements have then been completed with a 25 kHz transducer and a 2 MHz transducer, in both the laminar and the turbulent regimes.

2.3 Thermal approach

In the thermal approach, the objective is to analyze the influence of ultrasound on heat transfer and on the boundary layer. To achieve this aim, temperatures within the heating wall are measured using thermocouples, integrated into the heating blocks as described in section 2.1. It is then possible to quantify the convective heat transfer at each block, as a heat transfer coefficient h or a Nusselt number Nu. A heat transfer enhancement factor will also be defined to quantify the influence of ultrasound on heat transfer.

This section begins with a presentation of the protocol used for the temperature measurement, then describes the processing carried out on this experimental data to obtain a Nusselt number and an enhancement factor. This protocol is performed for different flow rates, ranging from 0.756 L.s^{-1} to 12.6 L.s^{-1}.

Recording starts with no ultrasound, when heating block temperatures are stable. The tests are divided into two phases. In the first phase, the temperatures are recorded for approximately 3 minutes in the absence of ultrasound. This time ensures that the average temperature for each measurement point is calculated over a large number of measurements. The ultrasound is then switched on, causing the temperature of the blocks to drop rapidly, qualitatively highlighting the increase of heat transfer. However, although more heat is transferred to the fluid, the temperature of the fluid does not increase significantly (about 0.1 °C), due to the high flow rate compared to the thermal power exchanged. The block temperatures gradually decrease after ultrasound activation, until they stabilize again. Temperature stabilization in the presence of ultrasound defines the beginning of the second recording phase for a duration of approximately 3 minutes. The average heating plate temperature for each regime (with and without ultrasound) is then calculated on both sides of each block (T_1 and T_2, see figure 1). This protocol has been carried out successfully in previous studies [10, 13].

Each test is performed 6 times under the same operating flow conditions, and the error bars are therefore the standard deviation, related to the reproducibility of the measurements. The average temperatures measured by thermocouples located on each side of the heating blocks (T_1 and T_2) allow to calculate the heat flow Φ (as previously stated, assumed to be unidirectional, according to x-axis) to be calculated between the measurement points T_1 and T_2 by application of the heat conduction law:

$$\Phi = k_{316L} \times S \times \frac{(T_1 - T_2)}{e_{T_1 - T_2}} \quad (2)$$

The wall temperature T_w is then estimated using the following formula, as the heat flow Φ is assumed to remain unidirectional and constant:

$$T_w = T_1 - \frac{\Phi \times e_{T_1 - T_w}}{k_{316L} \times S} \quad (3)$$

The convective heat transfer coefficient h [W.m^{-2}.K^{-1}] can then be calculated with T_{fluid} as the fluid temperature:

$$h = \frac{\Phi}{S \times (T_w - T_{fluid})} \quad (4)$$

Nusselt number, which represents the ratio between conductive and convective heat transfer within the fluid, is defined as:

$$Nu = \frac{h \times L_c}{k_{fluid}} \tag{5}$$

For a hydrodynamically developed internal flow, the characteristic length is the hydraulic diameter D_h. With a channel width d=33 mm, and a channel depth of 100 mm, the hydraulic diameter is 49.6 mm.

Then, a heat transfer enhancement factor HTEF is defined as a function of the heat transfer coefficients obtained under the same experimental conditions, without ultrasound h_{silent} and with ultrasound h_{US}:

$$HTEF = \frac{h_{us} - h_{silent}}{h_{silent}} \tag{6}$$

Finally, the analysis is performed with the thermal boundary layer thickness defined as the layer of fluid where heat transfer can be considered as diffusive only. Thus, the heat flux can be approximated as follows [29]:

$$\Phi \approx k_{fluid} \times S \times \frac{(T_w - T_{fluid})}{\delta_{th}} \tag{7}$$

It is important to note that this equation is only an approximation, since the temperature gradient within the boundary layer thickness is not linear. However, since the heat flow is only calculated at the boundaries of the thermal boundary layer (*i.e.*, at the surface of the heating plate T_w and the top of the boundary layer T_{fluid}), and not resolved across the entire boundary layer, it remains relevant for this analysis.

Finally, by combining equations (4) and (7), the thermal boundary layer thickness δ_{th} can therefore be evaluated as a function of the heat transfer coefficient h and the thermal conductivity k_{fluid} such that:

$$\delta_{th} \approx \frac{k_{fluid}}{h} \tag{8}$$

2.4 Test section characterization in silent conditions

Firstly, the test section was characterized hydrodynamically and thermally without ultrasound, with the aim of providing experimental results in silent conditions. Data was then used to validate the experimental set-up and procedure by comparing the results obtained to appropriate correlations.

2.4.1 Hydrodynamic characterization

Hydrodynamic characterization is carried out using PIV measurements to obtain velocity and TKE fields within the test section, without ultrasound. The measurements are performed for a flow rate of 0.756 L.s^{-1}, *i.e.*, a flow velocity U=0.018 m.s^{-1} and a Reynolds number of 890 (laminar regime), and for a flow rate of 8.6 L.s^{-1}, *i.e.*, a flow velocity U=0.2 m.s^{-1} and a Reynolds number of 10000 (turbulent regime). Regarding the development of the hydrodynamic boundary layer, the hydrodynamic entrance length can be determined from the following equation in the laminar regime [30]:

$$\frac{L_{e,lam}}{D_h} = 0.011 \cdot Re + \frac{0.315}{1 + 0.0175 \cdot Re} \tag{9}$$

And from the equation (10) in the turbulent regime [29]:

$$\frac{L_{e,turb}}{D_h} \approx 3.8 \cdot Re^{1/6} \tag{10}$$

Thus, for a Reynolds number equal to 890, the hydrodynamic entrance length is 0.49 m. For a Reynolds number equal to 10000, the hydrodynamic entrance length is 0.88 m. Thus, under these conditions, and for a channel width of d=33 mm, the flow within the test section is hydrodynamically developed for all the tests carried out.

Figure 4 presents the velocity profiles U_y (subfigure (a) and (b)) in the center of each heating block, and the TKE fields (subfigure (c) and (d)) for the two flow regimes studied. As a reminder, the ultrasonic transducer is located at x=33 mm and the heating plate at x=0 mm.

It is important to note that the design of the initial test section required a local wall recess of 3 mm, in order for the transducer to be mounted to the test section, as illustrated in figure 1. Consequently, it is not possible to measure the velocity field within this wall recess, as the laser sheet is not able to illuminate this area. This wall recess tends to interfere with the fluid flow between the transducer and the heating plate. As seen in both figure 4a and figure 4b, the velocity profile does not reach 0 $m.s^{-1}$ at x=-30 mm due to this wall recess. The theoretical models presented in each figure are also determined for a channel width of d=33 mm.

In the case of laminar flow (Re=890), the experimental velocity profiles (figure 4a) show a parabolic shape characteristic of a velocity profile in a flow between two parallel plates. The velocity profile represented as a red dotted line corresponds to the theoretical velocity profile in a flat rectangular pipe for a laminar flow, defined by the following equation [29]:

$$U_y(x) = \frac{3}{2} \cdot U \cdot \frac{(x^2 - d \cdot x)}{(0.5 \cdot d)^2} \tag{11}$$

Overall, the experimental results are consistent with the theoretical velocity profile. However, it is observed that the velocity profiles change as a function of the blocks. This modification can be explained by the presence of the wall recess at the transducer. This wall recess induces an increase in the cross-sectional area, and therefore a decrease in the flow velocity. This is reflected in a flattening of the velocity profile from block 1 to block 5. At block 5, the experimental results are very close to the theoretical results, as at this position the disturbance generated by the wall recess at the transducer no longer has significant effect on the heating plate.

For a turbulent flow (Re=10000) within the channel (figure 4b), the results show a logarithmic profile, as expected for a turbulent regime. However, it appears that the velocity measured near the heating wall (x=0 mm) is not zero. This is related to the limits of spatial resolution of the PIV measurements. Indeed, each measurement point corresponds to an interrogation window measuring 1.4 mm. However, in a turbulent flow, the velocity gradient is very high near the wall, and it is therefore more difficult to correctly measure a high velocity gradient at this resolution. It is observed again that the velocity profiles change as a function of the blocks, due to the change in cross-section, but in a much less marked way than in the laminar regime. The red dotted velocity profile corresponds to the theoretical velocity profile in a flat rectangular pipe for turbulent flow, known as the "1/7" power law and given by the following equation [29]:

$$U_y(x) = U \cdot \left(1 + 1.33 \cdot \sqrt{(100 \cdot Re_{D_h})^{-1/4}}\right) \cdot \frac{x}{0.5 \cdot d}^{1/7} \tag{12}$$

The theoretical velocity profile shows that the velocity gradient in the vicinity of the heating wall is indeed high. However, the experimental results are in close agreement with the theoretical profile, except for the area near the ultrasonic transducer (between x=-30 mm and x=-25 mm) where the deviation is larger due to the wall recess, as discussed above. The velocity profiles measured for each flow regime are therefore consistent with the theory, despite specific aspects of the design of the test section.

Regarding TKE fields in silent conditions, figure 4c shows that for a Reynolds number of 890, the measured TKE is close to 0 $m^2.s^{-2}$ within the measuring field. Since the flow

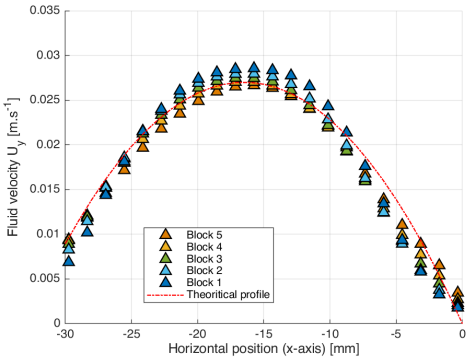

(a) U_y profile (Re=890)

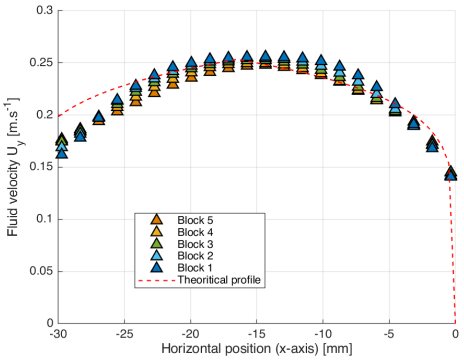

(b) U_y profile (Re=10000)

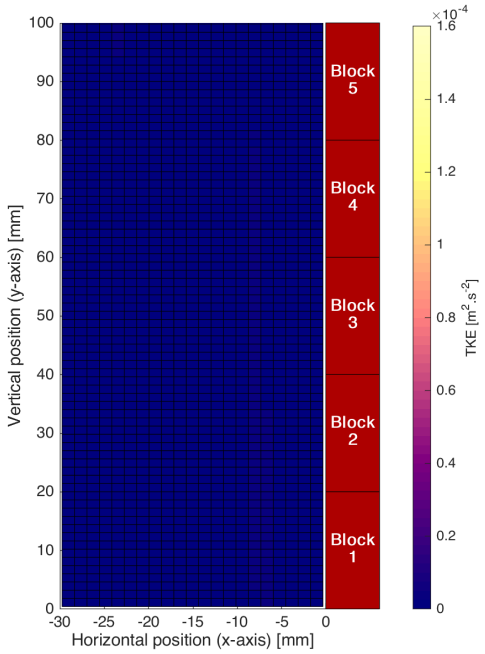

(c) TKE field (Re=890)

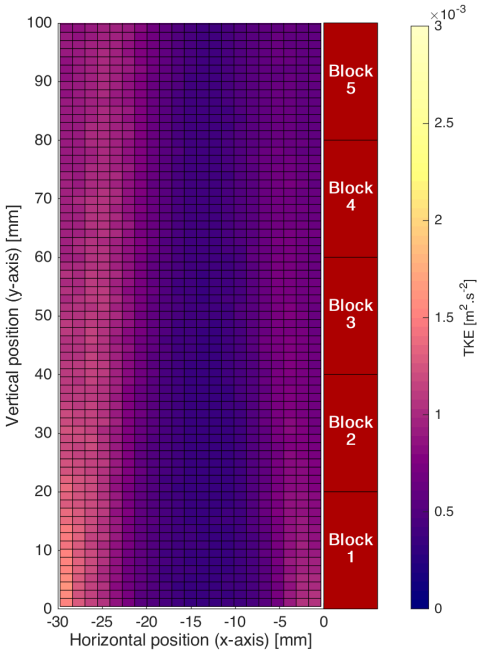

(d) TKE field (Re=10000)

Figure 4 – Hydrodynamic characterization for both flow regimes studied, without ultrasound. Channel width d=33 mm. (a) and (b): Experimental averaged velocity profiles U_y at each heating block and theoretical velocity profile, on x-axis. (c) and (d): TKE fields in the test section.

regime is laminar, it is indeed consistent to observe no fluctuation of the instantaneous velocity within the measurement field.

For a Reynolds number of 10000 (figure 4d), the TKE field shows values ranging from $0.3 \cdot 10^{-3}$ $m^2.s^{-2}$ to $1.6 \cdot 10^{-3}$ $m^2.s^{-2}$, with an average TKE in the measurement field of $0.7 \cdot 10^{-3}$ $m^2.s^{-2}$. The highest TKE values are observed near each wall, corresponding to the zone of interaction between the viscous sublayer, and the logarithmic zone where the production of turbulence is greatest. These results are thus consistent with the theory. However, an asymmetry is observed between the TKE values near the walls, with a higher TKE near the transducer (x=-30 mm) than near the heating wall (x=0 mm). This can again be explained again by the presence of the wall recess at the transducer, which induces local disturbance of the flow and thus generates instantaneous velocity fluctuations, resulting in higher TKE values near the wall recess.

Overall, the results obtained for the hydrodynamic characterization without ultrasound are consistent with the theoretical results expected for a rectangular, hydrodynamically developed channel, guaranteeing a controlled flow near the heating blocks. This step also provides reference data without ultrasound, with which the results obtained in the presence of ultrasound will be compared and an analysis made.

2.4.2 Thermal characterization

Thermal characterization is performed for a Reynolds number range of 890 to 14500, in order to assess how heat transfer changes as a function of the flow regime, without ultrasound. As previously described, the heat transfer within the test section is quantified using the temperature measurements taken within the heating blocks, leading to calculation of a heat transfer coefficient and thereby a Nusselt number at each heating block, following the methodology presented in section 2.3.

It is important to note that the flow is thermally non-fully developed, regardless of the flow rate. Indeed, since the heating plate is placed on a single wall of the channel, the thermal boundary layer must develop over the entire channel width. Thus, under the most favorable conditions (Re = 4000, *i.e.*, the smallest Reynolds number in the turbulent regime), the thermal entrance length is 1.95 m. Since the heating plate is 0.1 m long, the flow in this test section is thermally non-fully developed under all conditions.

Experimental results obtained with a channel width of d=33 mm are compared with results obtained from empirical correlations for internal hydrodynamically fully developed flow, and for thermally developing flow conditions. In laminar flow, the Nusselt number in a rectangular duct is a function of the dimensionless axial position in the thermal entrance region, named y^*, defined as:

$$y^* = \frac{y}{D_h} \cdot \frac{1}{Re \cdot Pr} \tag{13}$$

The Nusselt number can then be calculated from the following correlation for a plane, thermally developing flow with uniform heat flux, valid for $y^* < 0.001$ [30]:

$$Nu = 2.236 \cdot (y^*)^{-1/3} \tag{14}$$

For turbulent flow in a rectangular pipe, in order to use the correlations for circular pipes, the hydraulic diameter was used. For a hydrodynamically and thermally developed flow, the Gnielinski correlation, valid for $1.5 \leq Pr \leq 500$ and $3000 \leq Re \leq 10^6$ [30], was used:

$$Nu_\infty = 0.012 \cdot (Re^{0.87} - 280) \cdot Pr^{0,4} \tag{15}$$

In the case of thermally developing flow, it is possible to use the following correction of the Nusselt number, valid for $y/D_h \geq 2$; $0.7 \leq Pr \leq 75$ and $3500 \leq Re \leq 10^5$ [30]:

$$Nu = (1 + \frac{C}{y/D_h}) \cdot Nu_\infty \tag{16}$$

with C defined as:

$$C = \frac{(y/D_h)^{0.1}}{Pr^{1/6}} \cdot (0.68 + \frac{3000}{Re^{0.81}}) \tag{17}$$

In order to analyze how the convective heat transfer in silent conditions varies as a function of the flow regime, figure 5 presents the change in the Nusselt number as a function of the Reynolds number, for all the tests performed. These results are presented for the position where the thermal boundary layer is most developed, *i.e.*, at block 5. The results can be compared to those of corresponding empirical correlations according to their respective domains of validity, as described previously.

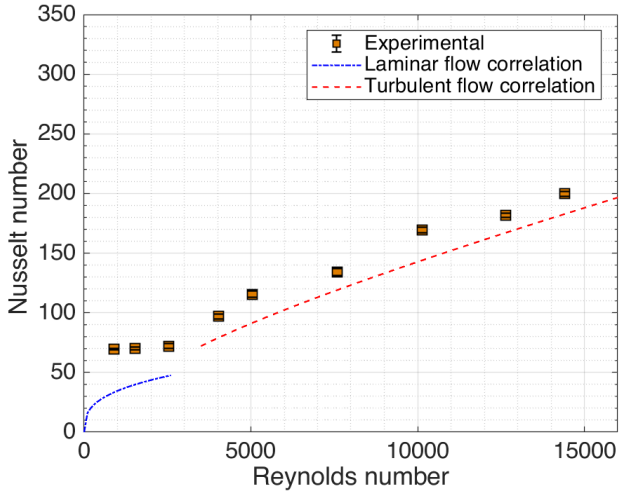

Figure 5 – Nusselt number without ultrasound as a function of the Reynolds number, from laminar to turbulent flow. Channel width $d = 33\ mm$.

The experimental results show an increase in the Nusselt number as the Reynolds number increases, following a trend similar to those obtained from empirical correlations. The thermal characterization of the test section without ultrasound confirms that the experimental results are consistent with the theory, over a range of Reynolds numbers from 890 to 14500. Nevertheless, some deviations are observed between experimental results and empirical correlations, especially in the laminar regime. This deviation can be explained by the presence of wall recess, as it has been previously shown that the wall recess induces some disturbance of the velocity profile, and could therefore induce a slightly higher convective heat transfer. However, this deviation remains constant regardless of the Reynolds number. Moreover, given the uncertainties in the experimental results and from empirical expressions, it seems reasonable to assume that they remain comparable. Thus, this thermal characterization without ultrasound provides a reference state under silent conditions for this study, with which the results in the presence of ultrasound will be compared.

3 Results and discussion

This section presents the results obtained in this work and the analysis that can be drawn from them. The first part is dedicated to studying the influence of the flow regime on ultrasound effects, for both frequencies, and looking at hydrodynamic effects and thermal effects.

The second part provides an analysis of the heat transfer enhancement induced by ultrasound with respect to the initial boundary layer thickness in silent conditions.

3.1 Flow regime influence with constant channel width

3.1.1 Hydrodynamic study in the presence of low frequency ultrasound

Firstly, the influence of low frequency ultrasound on hydrodynamics is analyzed as a function of the flow regime. As mentioned previously, acoustic cavitation can be generated with the 25 kHz transducer used in this study.

Implementing a hydrodynamic approach, in this section an analysis of the effects of 25 kHz ultrasound is carried out with respect to its influence on the mean velocity field within the flow, as well as on the instantaneous velocity fluctuations generated by ultrasound, from the Turbulent Kinetic Energy (TKE). This analysis is performed under two flow regimes: laminar (Re=890) and turbulent (Re=10000).

In order to quantify the influence of ultrasound on the streamwise averaged velocity U_y within the channel for both flow regimes, the ratio U_{us}/U_{silent} between velocity fields obtained with ultrasound and in silent conditions is presented in figure 6. The scale is colored so that when ultrasound produces a decrease in velocity, the color of the field tends towards blue, while when it induces an increase in velocity, the color of the field tends towards red. When the velocity is not affected by ultrasound, the field color remains white.

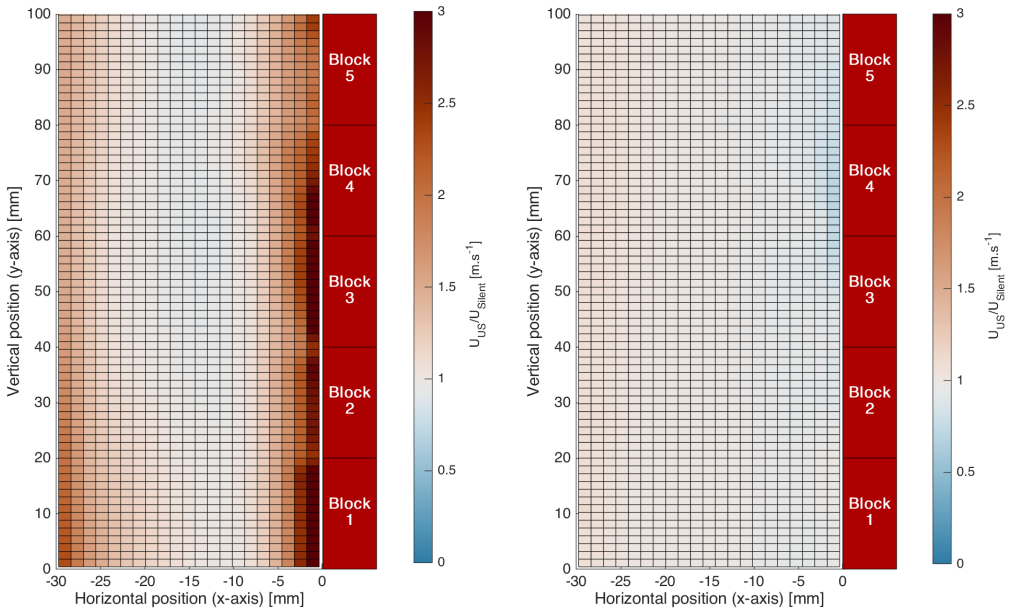

(a) Laminar regime (Re=890) (b) Turbulent regime (Re=10000)

Figure 6 – Ratio between averaged velocity fields U_y obtained with and without ultrasound in the test section, for both flow regimes. (Channel width d=33 mm, f_{us} = 25 kHz, P_{us} = 110 W).

Figure 6a shows that in the laminar regime (Re = 890), ultrasound induces an increase

in velocity near the walls, and a slight decrease in velocity in the center of the channel. It highlights that low frequency ultrasound induces an increase in the velocity gradient near the walls. Since the parietal shear stress is a function of the velocity gradient and the dynamic viscosity, which is assumed here to be constant, 25 kHz ultrasound therefore increases the parietal shear stress along both the heating wall and the emitter, for the laminar regime.

For a Reynolds number of 10000, Figure 6b shows that the effects of 25 kHz ultrasound are less significant on the velocity field, since the velocity field ratio is close to 1. However, a slight decrease of the velocity in the channel is observed, with a velocity ratio between 0.8 and 1. Previous results by Nomura *et al.* (2002) [8] also succinctly showed that the effects of low frequency ultrasound on the velocity profile of the flow were less significant for a Reynolds number of 4000 than for a Reynolds number of 1500. The results presented here also illustrate that in the turbulent regime, low frequency ultrasound no longer has a significant effect on the velocity field.

Thus, the 25 kHz ultrasound, thanks to induced acoustic cavitation, can strongly perturb the U_y velocity field in the laminar regime, by inducing an increase of the velocity near the walls, and thus an increase of the momentum transfer. However, ultrasound effects are much less pronounced on the U_y velocity field in the turbulent regime.

The influence of 25 kHz ultrasound on the instantaneous velocity fluctuations, in both the laminar and turbulent regime, can be analyzed by means of TKE fields (figure 7) and compared to results observed without ultrasound (figures 4c and 4d).

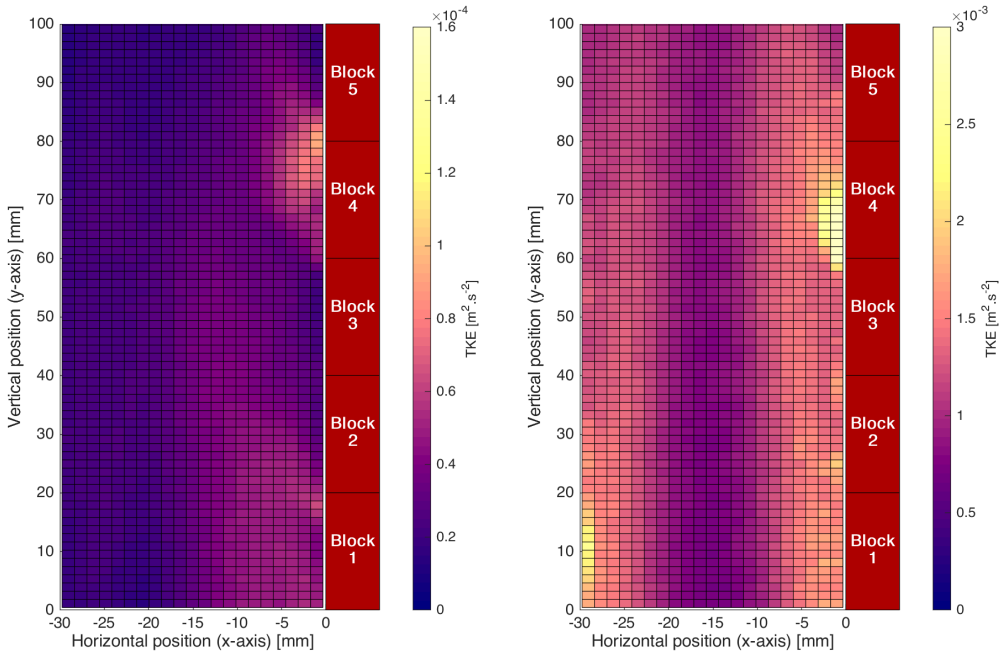

(a) Laminar regime (Re=890) (b) Turbulent regime (Re=10000)

Figure 7 – TKE fields in the test section for both flow regimes studied, with low-frequency ultrasound. (Channel width d=33 mm, f_{us} = 25 kHz, P_{us} = 110 W).

In the laminar regime (figure 7a), the presence of acoustic cavitation induced by 25 kHz ultrasound causes the generation of turbulent kinetic energy (TKE), with values ranging from $0.15 \cdot 10^{-4}$ $m^2.s^{-2}$ to $0.93 \cdot 10^{-4}$ $m^2.s^{-2}$. The average TKE in the whole measurement field is $0.32 \cdot 10^{-4}$ $m^2.s^{-2}$ in the presence of ultrasound, while figure 4c gives an average TKE of $0 \cdot 10^{-4}$ $m^2.s^{-2}$ in silent conditions. The TKE distribution is quite homogeneous near the heating wall, with some very localized areas where the values are higher. The highest TKE values are measured near the heating wall, specifically at blocks 1 and 2,

and between blocks 4 and 5. Acoustic cavitation is at the origin of the turbulent kinetic energy generation at the wall opposite the emitter, as cavitation bubbles collapse generates high velocity micro-jet of fluid, and thus inducing local instantaneous velocity fluctuations. These instantaneous velocity fluctuations are therefore at the origin of the observed increase the turbulent kinetic energy. These results are thus similar to the results seen in other works in the literature [8, 10, 24], which have also shown turbulent kinetic energy in laminar flow in the presence of 25 kHz ultrasound, thus confirming the consistency of these observations.

In the turbulent regime (figure 7b), ultrasound again induces an increase of TKE within the measurement field, compared to the results without ultrasound (figure 4d), but with lower enhancement compared to the laminar flow results. The average TKE is $1.2 \cdot 10^{-3}\ m^2.s^{-2}$, compared to $0.7 \cdot 10^{-3}\ m^2.s^{-2}$ in silent conditions. The highest TKE values are found near the heated wall, similar to the results obtained with laminar flow. These results are thus consistent with those of Bulliard *et al.* (2019) [10] who showed that 25 kHz ultrasound mainly induce an increase in TKE near the wall as the Reynolds number increase. It is important to note that for figure 7b, some interrogation windows show significantly higher values than others, and are therefore presented as saturated. Since these interrogation windows are close to the wall, there is a high possibility that these values are related to measurement errors.

These results demonstrate that in the turbulent regime, despite a very negligible influence on the mean velocity field, the acoustic cavitation generated by 25 kHz ultrasound induces an increase of the turbulent kinetic energy in an already turbulent flow. Therefore, while 25 kHz ultrasound in the turbulent regime may induce instantaneous velocity fluctuations, it does not influence the average velocity field of the flow.

3.1.2 Thermal study in the presence of low frequency ultrasound

Having analyzed the hydrodynamic effects of acoustic cavitation on the water flow in the above, this section now focuses on an analysis of the effects of 25 kHz ultrasound on convective heat transfer, as a function of the flow regime.

In order to evaluate the effects of the flow regime on heat transfer in the presence of low frequency ultrasound, figure 8 shows the changes in the Nusselt number at block 5 with and without ultrasound (f = 25 kHz), as a function of the Reynolds number.

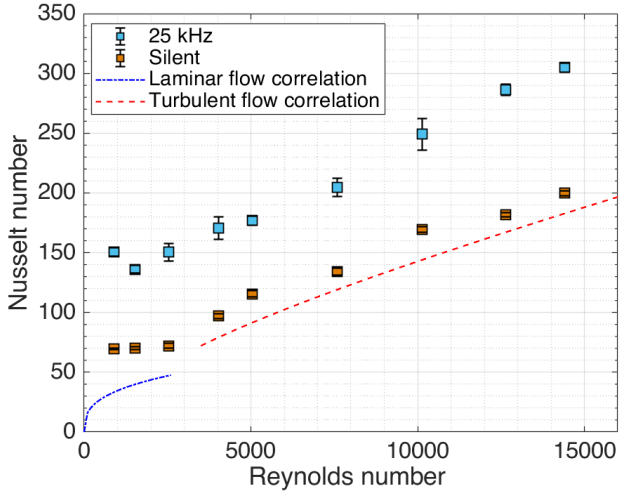

Figure 8 – Nusselt number at block 5 ($y = 90.6\ mm$) as a function of the Reynolds number, from laminar to turbulent flow. (Channel width $d = 33\ mm$, $f_{us} = 25$ kHz, $P_{us} = 110$ W).

The results clearly show that for a given Reynolds number, the Nusselt number obtained with 25 kHz ultrasound is always higher than without ultrasound, regardless of the flow regime.

In silent conditions, the increase in Reynolds number implies a decrease in the thickness of the thermal boundary layer and thus an improvement in convective heat transfer, quantified by the increasing Nusselt number. Generation of 25 kHz ultrasound within the flow induces an increase in Nusselt number for a given Reynolds number. Therefore, one can assume that 25 kHz ultrasound will lead to disturbance of the boundary layer and enhanced convective heat transfer.

Indeed, hydrodynamic analysis has shown that for laminar flow, 25 kHz ultrasound induces disturbance of the mean velocity profiles, with a larger velocity gradient near the heating wall and the generation of turbulent kinetic energy. The hydrodynamic effects induced by acoustic cavitation produced by 25 kHz ultrasound thus increase the parietal shear stress, and the results given here show that the convective heat transfer is consequently increased.

For turbulent flow, the hydrodynamic analysis has shown that ultrasound had a negligible effect on the mean velocity profiles. Furthermore, although turbulent kinetic energy increases in the presence of 25 kHz ultrasound in the turbulent regime, this increase is less significant than for the laminar regime. The convective effects measured by PIV are thus lower. However, the thermal results illustrate that 25 kHz ultrasound still significantly increases the parietal heat transfer in the turbulent regime.

These results are consistent with the analysis provided by Barthès *et al.* (2015) [11] who reported that the increase in the Reynolds number induces dissipation of the convective effects produced by ultrasound. However, mass transfer at the wall measured in front of the ultrasound transmitter remains higher in the presence of ultrasound, even in the turbulent regime, while the convective effects near the wall are largely dissipated. The authors thus concluded that the hydrodynamic effects associated with the implosion of the acoustic cavitation bubbles at a microscopic scale lead to an improvement in mass transfer at the wall opposite the ultrasonic emitter, independent of the absence of significant convective effects of ultrasound on the flow at a macroscopic scale.

In this case, acoustic cavitation results in increased heat transfer at the heating wall, and thus in a higher Nusselt number than without ultrasound, regardless of the Reynolds number, despite the fact that the hydrodynamic effects at the macroscopic scale are less significant in the turbulent regime.

To summarize, the increased convective heat transfer can be explained by the hydrodynamic effects of acoustic cavitation generated within the flow, associated with the thermal boundary layer disruption generated by the acoustic bubble collapse occuring near the heating wall.

In order to quantify the heat transfer enhancement induced by ultrasound, a heat transfer enhancement factor (HTEF, according to equation (6)) can be determined from the heat transfer coefficient without and with ultrasound. Figure 9 shows the variation in the HTEF obtained with 25 kHz ultrasound as a function of the Reynolds number.

Figure 9 shows that in the laminar regime the HTEF remains between 110% to 120%. The HTEF decreases sharply for Reynolds numbers above 2500 and then reaches an asymptote, with an HTEF of about 50% for Reynolds numbers above 10000. The heat transfer enhancement produced by ultrasound thus varies as a function of the flow regime. This variation is similar to that observed by Legay *et al.* (2012) [21] who measured significant heat transfer enhancement in the laminar regime with low frequency ultrasound in a double-tube heat exchanger, followed by a decrease in heat transfer enhancement with increasing Reynolds number, until the heat transfer enhancement stabilized.

According to these results, some conclusions can be drawn regarding the influence of 25 kHz ultrasound. In laminar flow, 25 kHz ultrasound generates disturbance in the velocity profiles, and induces a larger velocity gradient near the heating wall which in turn means the parietal shear stress increases. In addition, 25 kHz ultrasound generates instantaneous velocity fluctuations within the flow, quantified through the turbulent kinetic energy. These effects on the parietal shear stress are also observed on heat transfer, since

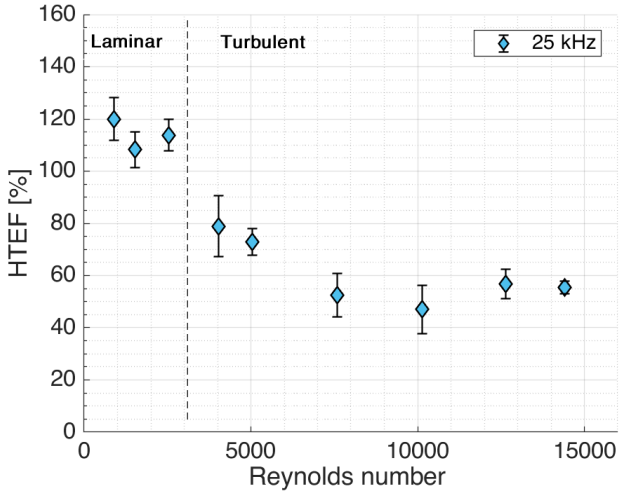

Figure 9 – Heat Transfer Enhancement Factor at block 5 ($y = 90.6\ mm$) as a function of the Reynolds number, from laminar to turbulent flow. (Channel width $d = 33\ mm$, $f_{us} = 25$ kHz, $P_{us} = 110$ W).

in the laminar regime ultrasound leads to heat transfer enhancement.

In the turbulent regime, 25 kHz ultrasound has almost no effect on the velocity profiles. However, it contributes to an increase in the turbulent kinetic energy, but to a lesser extent compared to the laminar regime. Thus, in the turbulent regime, the convective effects of 25 kHz ultrasound are significantly reduced. However, hydrodynamic effects induced by acoustic cavitation are sufficient to ensure an enhancement of heat transfer at the wall surface, although this enhancement is lower than in the laminar regime.

As a conclusion, 25 kHz ultrasound ensures significant heat transfer enhancement over the entire Reynolds range studied in this work.

3.1.3 Hydrodynamic study in the presence of high frequency ultrasound

This second part is dedicated studying of the influence of high frequency ultrasound on hydrodynamics as a function of flow regime. As previously stated, 2 MHz ultrasound used in this study results mainly in acoustic streaming. The effects produced by 2 MHz ultrasound are first analyzed from PIV measurements, under two different flow regimes, in a similar way to the analysis presented for 25 kHz ultrasound. PIV measurements will be used to study the influence of 2 MHz ultrasound on velocity profiles and on turbulent kinetic energy fields.

Figure 10 shows the ratio between the streamwise averaged velocity fields obtained with high frequency ultrasound and in silent conditions U_{us}/U_{silent}.

Figure 10a clearly demonstrates that 2 MHz ultrasound induces a significant decrease in velocity ($U_{us}/U_{silent} < 1$) in the area near the ultrasound transducer. This zone of decreased velocity widens along the channel, representing about 6 mm (between $x = -30\ mm$ and $x = -24\ mm$) at block 1 ($y = 10\ mm$), and about 16 mm (between $x = -30\ mm$ and $x = -14\ mm$) at block 4 ($y = 70\ mm$). Thus, the acoustic streaming produced by 2 MHz ultrasound, generated perpendicular to the water flow, behaves as if it was forming an obstacle to the flow, resulting in a smaller cross-sectional area for the fluid flow. At constant flow rate, this implies an increase in velocity near the heating wall, where the acoustic streaming does not influence the flow, and thus an increase in the parietal shear stress.

In the turbulent regime, figure 10b highlights that the influence of 2 MHz ultrasound on the velocity U_y is negligible in the whole measurement field. Indeed, it seems that acoustic streaming generated by 2 MHz ultrasound no longer has influence on the U_y averaged

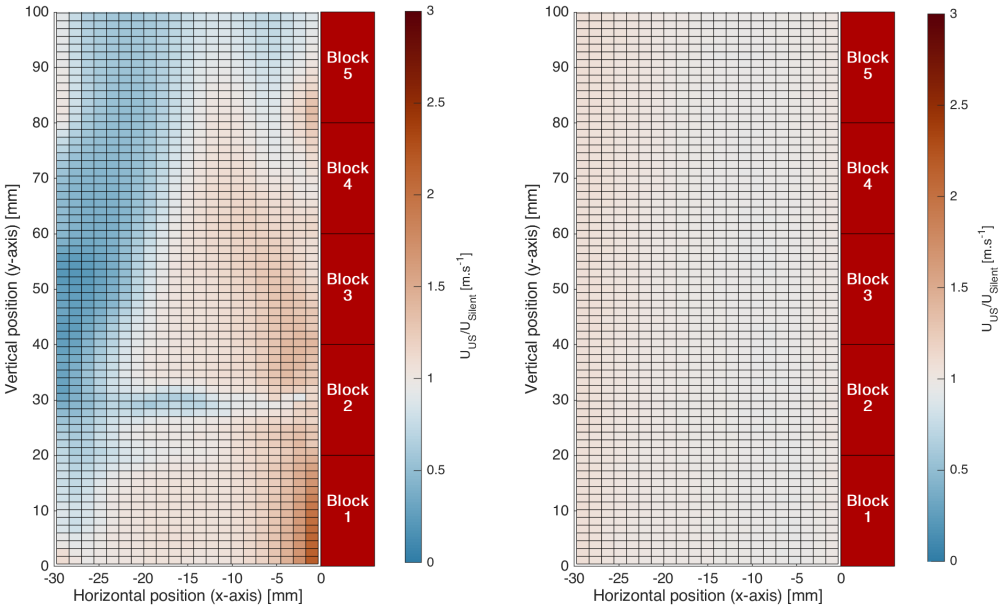

(a) Laminar regime (Re=890)

(b) Turbulent regime (Re=10000)

Figure 10 – Ratio between averaged velocity fields U_y obtained with and without ultrasound in the test section, for both flow regimes. (Channel width $d = 33\ mm$, $f_{us} = 2$ MHz, $P_{us} = 110$ W).

velocity field, as the velocity of the fluid is much higher than the acoustic streaming velocity. Consequently, the average convective effects of ultrasound are thus largely dissipated.

Figure 11 illustrates the turbulent kinetic energy fields (TKE) obtained with 2 MHz ultrasound for both flow regimes studied.

In the laminar regime, (figure 11a), the TKE values range from $0.05 \cdot 10^{-4}\ m^2.s^{-2}$ to $1.6 \cdot 10^{-4}\ m^2.s^{-2}$. The average TKE over the entire measurement field is $0.3 \cdot 10^{-4}\ m^2.s^{-2}$. For this flow regime, the TKE field shows significant similarity with figure 10a, since the areas where the TKE is highest correspond to the areas where the ratio U_{us}/U_{Silent} is close to 1. It is also observed that the TKE is highest in the center of the flow at block 2 ($y \approx 30\ mm$).

In the laminar regime, these results show that acoustic streaming generated perpendicular to the flow, induces perturbations of the flow, both on the average velocity profile, as seen previously, and on instantaneous velocity fields, which results in the presence of turbulent kinetic energy within the flow. As it can be seen with these PIV results in laminar regime, the velocity fluctuations causing the turbulent kinetic energy are largest in the area of interaction between the water flow and the acoustic streaming.

Figure 11b shows the TKE field in the turbulent regime. The TKE values range from $0.5 \cdot 10^{-3}\ m^2.s^{-2}$ to $2.5 \cdot 10^{-3}\ m^2.s^{-2}$. The average TKE in the entire measurement field of the test section is $1 \cdot 10^{-3}\ m^2.s^{-2}$ compared to $0.7 \cdot 10^{-3}\ m^2.s^{-2}$ in silent conditions. Thus, 2 MHz ultrasound induces a small increase in turbulent kinetic energy compared to silent conditions, for the same Reynolds number.

Therefore, 2 MHz ultrasound induces effects which vary greatly as a function of the flow regime. Indeed, in laminar flow, the acoustic streaming produced by ultrasound induces a significant perturbation of the average velocity field, which results in a significant decrease of the velocity U_y near the ultrasonic transducer. Since the flow rate is constant, the velocity U_y increases near the opposite side of the channel, *i.e.*, near the heating wall. It is important to note that the velocity increase could also be partly in the U_z component, due to anisotropic effects. However, these could not have been taken into account here, due to

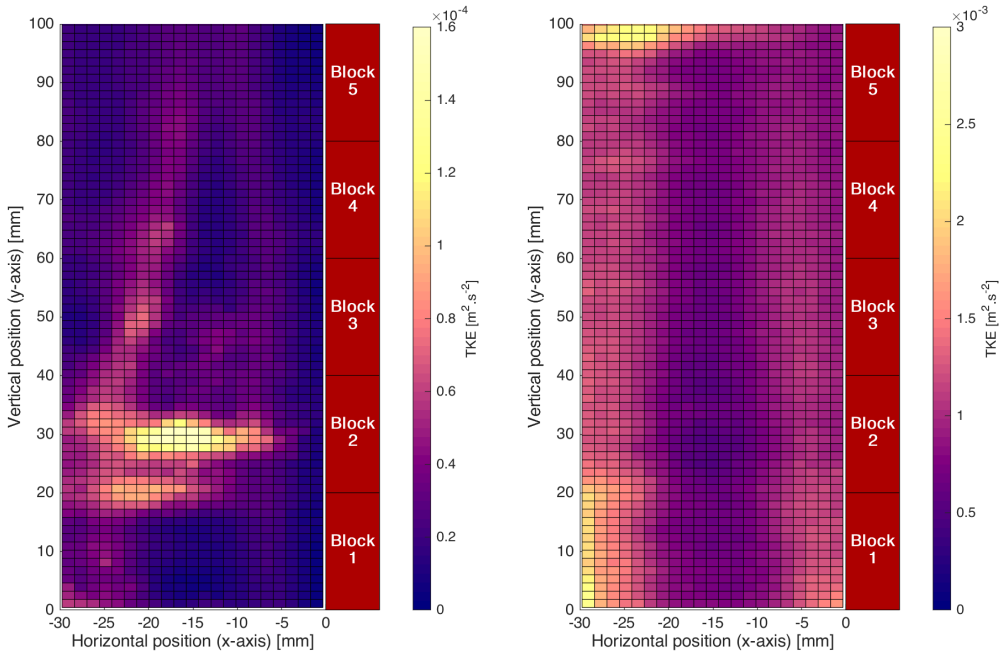

(a) Re = 890 (b) Re = 10000

Figure 11 – TKE fields in the test section, for both flow regimes studied, with 2 MHz ultrasound. (Channel width $d = 33\ mm$, f_{us} = 2 MHz, P_{us} = 110 W).

the 2D-2C PIV device used in this work. The areas of interaction between the acoustic streaming produced by 2 MHz ultrasound and the water flow also correspond to the areas of strong velocity fluctuations, which result in the production of turbulent kinetic energy within a laminar flow.

When 2 MHz ultrasound is generated in a turbulent flow, the induced effects are less significant. Indeed, acoustic streaming does not produce any significant effect on the velocity field. The results show that nevertheless it does cause a slight increase in the turbulent kinetic energy within the flow. However, the inertial forces of the flow contributes much more to generating turbulence than the2 MHz ultrasound. Thus, 2 MHz ultrasound produces significant convective effects when the flow regime is laminar. These effects are considerably attenuated when the flow regime is turbulent.

3.1.4 Thermal study in the presence of high frequency ultrasound

After analyzing the effects of acoustic streaming on the hydrodynamics of fluid flow, the aim of this section is to analyze variation in the effects of acoustic streaming on heat transfer as a function of the flow regime.

To do so, figure 12 shows the change in Nusselt number at block 5, without ultrasound, and with 2 MHz ultrasound, as a function of the Reynolds number.

As shown in figure 12, the Nusselt number remains constant overall with 2 MHz ultrasound, at about 140 ±10, for Reynolds numbers between 890 and 7500. Above this Reynolds interval, in silent conditions, the Nusselt number increases with the Reynolds number, as described previously. Thus, the difference between the Nusselt numbers obtained with and without 2 MHz ultrasound reduces as the Reynolds number increases. Above a Reynolds number of 7500, the Nusselt number with 2 MHz ultrasound is identical to the Nusselt number without ultrasound and follows the same increasing trend as a function of the Reynolds number.

As mentioned previously, 2 MHz ultrasound induces acoustic streaming, here generated

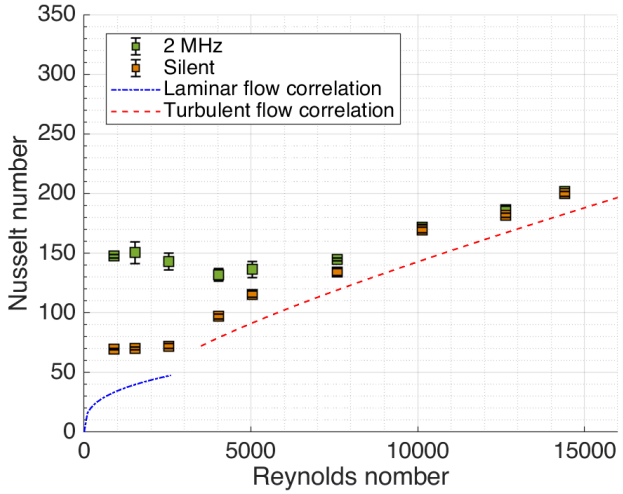

Figure 12 – Nusselt number at block 5 ($y = 90.6\ mm$) as a function of the Reynolds number, from laminar to turbulent flow. (Channel width $d = 33\ mm$, $f_{us} = 2$ MHz, $P_{us} = 110$ W).

perpendicular to the flow. Consequently, the velocity profile is disturbed, as depicted on figure 10a, thermal boundary layer is reduced and convective heat transfer increases. However, the convective heat transfer in presence of 2 MHz ultrasound for Reynolds number between of 890 and 7500 tends to slightly decrease. Indeed, acoustic streaming generated perpendicular to the main flow, which can be compared to a fluid jet, undergo a deflecting effect due to the increase of flowrate, reducing its influence on the heating wall and thus preventing the acoustic streaming from disturbing the boundary layer. However, above a Reynolds number of 7500, the flow without ultrasound induces a thermal boundary layer thin enough that acoustic streaming induced by 2 MHz ultrasound cannot disturb it. Therefore, beyond this Reynolds number, 2 MHz ultrasound does not have any influence on heat transfer.

Thus 2 MHz ultrasound ensures a higher convective heat transfer than without ultrasound in this case, as long as the Nusselt number induced by the hydrodynamic conditions is below 150.

The heat transfer enhancement factor (HTEF) obtained in the presence of 2 MHz ultrasound is shown in Figure 13 as a function of the Reynolds number.

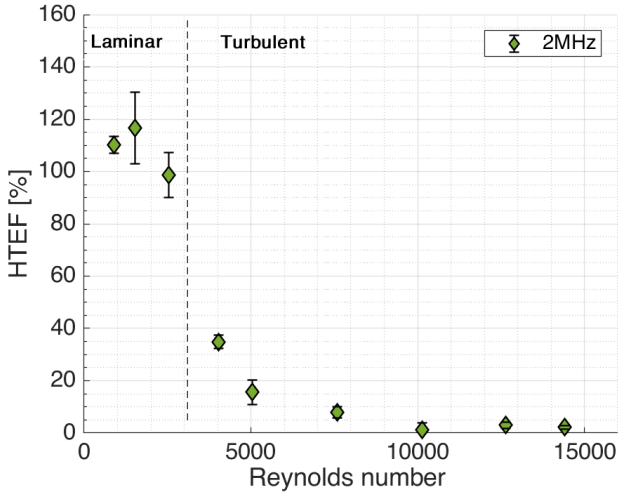

Figure 13 – Heat Transfer Enhancement Factor at block 5 ($y = 90.6\ mm$) as a function of the Reynolds number, from laminar to turbulent flow. (Channel width $d = 33\ mm$, $f_{us} = 2$ MHz, $P_{us} = 110$ W).

It can be seen that the HTEF in the laminar regime ranges between 95% and 110%. The enhancement factor then decreases rapidly for Reynolds numbers above 2500, until it reaches a value close to 0% for Reynolds numbers above 7500. Therefore, one might consider here that no enhancement of heat transfer is induced by 2 MHz ultrasound above this Reynolds number. This trend was partly observed by Bulliard *et al.* (2017) [13], however, their results did not lead to identification of a Reynolds number threshold beyond which 2 MHz ultrasound no longer induces enhancement of the heat transfer.

To summarize, the hydrodynamic analysis showed that acoustic streaming produced by 2 MHz ultrasound can cause perturbation of velocity profiles within a laminar flow, and thereby increase the turbulent kinetic energy. However, the convective effects of ultrasound are greatly reduced when the flow becomes turbulent, as the velocity profiles are not modified by the presence of 2 MHz ultrasound, and the turbulent kinetic energy does not increase substantially. As acoustic streaming is identified as the main heat transfer enhancement vector with high frequency ultrasound [13,31,32], dissipation of these convective effects results in an attenuation and cancellation of the heat transfer enhancement.

In conclusion, the use of 2 MHz ultrasound to enhance heat transfer, with this ultrasonic power and for this test section, remains of interest only for a limited to a Reynolds number range up to 7500. Beyond this range, ultrasound no longer generates any heat transfer enhancement, and is therefore no longer of interest for higher Reynolds numbers where the heat transfer level is naturally already high under silent conditions.

3.2 Analysis from the thermal boundary layer perspective

As stated in the above, since the flow along the heating plate is thermally developing, the HTEF values as a function of the Reynolds number are only valid for a single position on the heating plate. However, the results obtained with temperature measurements allow to evaluate the thermal boundary layer thickness in silent regime (initial thermal boundary layer) from different locations on the plate (5 blocks) and at different flow rates. Indeed, to characterize the thermal boundary layer thickness, the inverse of the heat transfer coefficient obtained without ultrasound h_{silent} can be used, which corresponds to the thermal resistance of the initial thermal boundary layer along the heating wall. This ratio $1/h_{silent}$ is here related to the thickness of the initial thermal boundary layer, as shown by equation (8) since all the tests were carried out with the same fluid and at the same temperature, the thermal conductivity k of the fluid therefore remains unchanged. Consequently, the data from experimental results for different channel widths d and Reynolds number provide a large range of thermal boundary layer thickness in silent regime, and the HTEF obtained with the initial thermal boundary layer thickness. Therefore, in order to compare HTEF values for different positions on the heating plate, the boundary layer thickness is introduced as a relevant parameter to compare these results, independently of the position and Reynolds number. The analysis of heat transfer enhancement is thus based on thermal boundary layer thickness. Initially, it focuses on results obtained with a channel width of d=33 mm, and it is subsequently extended to include three different channel widths, d=33 mm, d=63 mm and d=107.5 mm respectively.

3.2.1 Heat transfer enhancement with a fixed channel width

This first section deals with analysis of the heat transfer enhancement induced by ultrasound, using a constant channel width $d = 33\ mm$, as a function of the thermal resistance of the initial thermal boundary layer thickness.

Figure 14 shows the variation of HTEF as a function of the inverse of the heat transfer coefficient in silent conditions for all heating blocks. This analysis, despite being only qualitative, does provide a basis for analysis of variation in the heat transfer enhancement as a function of the initial thermal boundary layer.

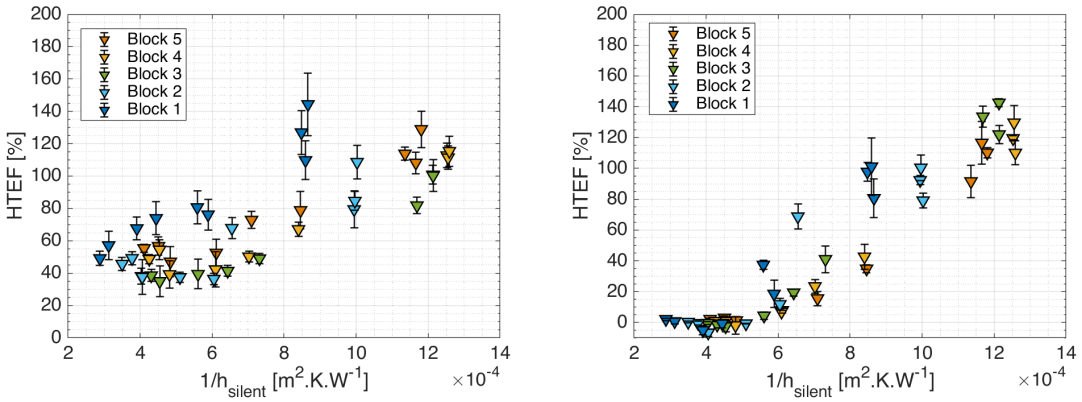

(a) f_{us} = 25 kHz (b) f_{us} = 2 MHz

Figure 14 – Heat Transfer Enhancement Factor as a function of estimated thermal resistance of the initial thermal boundary layer (Channel width $d = 33\ mm$, P_{us} = 110 W).

Figure 14a shows that in the presence of 25 kHz ultrasound, the heat transfer enhancement increases as the boundary layer thickness in the silent regime increases, regardless of the heating blocks considered. Indeed, the variation in the HTEF is similar for all the blocks, except for block 1, for which the HTEF is higher overall, regardless of the thickness of the thermal boundary layer. These results on block 1 can be explained by the fact that the ultrasonic field might be poorly distributed with this 25 kHz ultrasonic transducer, due to the geometrical configuration of piezoelectric ceramics. Consequently, inhomogeneous cavitation is generated and might have a greater impact on block 1 than on the other blocks.

These results are thus consistent with the general observations for heat transfer enhancement by ultrasound. Indeed, in forced convection, an increase of the flow velocity or more generally of the Reynolds number induces a reduction in the thermal boundary layer. Several works have shown that heat transfer enhancement produced by ultrasound tends to decrease with increasing flow regime [23, 33, 34]. But the results are also consistent with the results obtained in natural convection. Indeed, as shown in the bibliography, heat transfer enhancement generated by ultrasound decreases with an increase in the heat flux [16, 32, 35], *i.e.*, a reduction of the boundary layer thickness.

As shown in figure 14b, overall the results are aggregated regardless of the block considered, defining an overall trend. Thus, the heat transfer enhancement caused by the use of 2 MHz ultrasound increases rapidly as the boundary layer thickness increases. On the other hand, the absence of enhancement is very clear below a given boundary layer thickness.

Therefore, acoustic streaming produced by 2 MHz ultrasound enhances heat transfer and reduces the thermal boundary layer up to a certain initial thickness, whose thermal resistance is estimated here to be $1/h_{silent} = 5 \cdot 10^{-4}\ m^2.K.W^{-1}$. If flow without ultrasound induces a thermal boundary layer with thermal resistance below this threshold value, acoustic streaming no longer influences this thermal boundary layer, and is therefore not able to increase heat transfer. Heat transfer is then only driven by hydrodynamics of the flow in silent conditions and the presence of high frequency ultrasound is no longer of any interest for heat transfer enhancement.

3.2.2 Heat transfer enhancement with three different channel widths

This second section aims to analyze heat transfer enhancement with ultrasound in different hydrodynamic configurations, based on modification of the channel width d, *i.e.*, the distance between the ultrasonic transducer and the heating plate. In this section, the measurements were carried out in the same test section, but with two additional channel

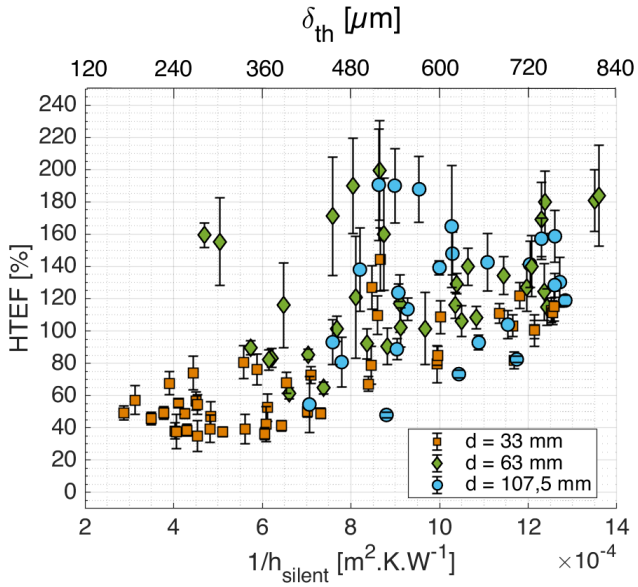

Figure 15 – Heat Transfer Enhancement Factor as a function of initial thermal resistance and corresponding estimated thermal boundary layer thickness for the three channel widths (f_{us} = 25 kHz, P_{us} = 110 W).

widths $d = 63\ mm$ and $d = 107.5\ mm$, progressively tending towards a heat transfer mode driven by external forced convection instead of internal forced convection obtained with the $d = 33\ mm$ channel width.

The objective here is to compare the results obtained for each of the channel widths. However, it is not possible to use dimensionless quantities such as Nusselt and Reynolds numbers due to the different types of flows (internal and external). Thus, heat transfer enhancement can be analyzed from the HTEF as a function of the inverse of the heat transfer coefficient, corresponding to the thermal resistance of the initial thermal boundary layer.

All HTEF values are given in figures 15 and 16, for 25 kHz ultrasound and 2 MHz ultrasound respectively. They are presented as a function of the inverse of the heat transfer coefficient without ultrasound ($1/h_{silent}$), combined with the thermal boundary layer thickness for all the heating blocks, and in terms of the three different channel widths d studied.

As shown on both figures 15 and 16, the heat transfer enhancement factor increases as the ratio $1/h_{silent}$ increases, regardless of the channel width. It is also observed that for fixed values of $1/h_{silent}$, the observed heat transfer enhancement is similar for all the channel widths in both figures. This observation suggests that heat transfer enhancement produced by ultrasound depends only on the initial thickness of the thermal boundary layer in silent conditions and not on the channel width. This also means that this variation is independent of the type of forced convection that is at work (internal or external).

However, it is important to note that the HTEF values can be quite scattered, especially for channel width $d = 107.5\ mm$, and that some values have large standard deviations. Indeed, as shown on figure 15, acoustic cavitation results in significant heat transfer enhancement, however the stochastic nature of acoustic cavitation can induce notable differences from one test to another, resulting in large standard deviations. Furthermore, the HTEF values at block 1 on the heating plate tend to be higher than the others, and show large standard deviations, regardless of the channel width d used, which could be due to inhomogeneous cavitation generated by the transducer around block 1.

It is also important to note that for 25 kHz ultrasound, the minimum value reached by the HTEF (thus corresponding to the minimum thermal boundary layer thickness) is 40%, for $1/h_{silent}$ below $6 \cdot 10^{-4}\ m^2.K.W^{-1}$. For water, with a thermal conductivity of

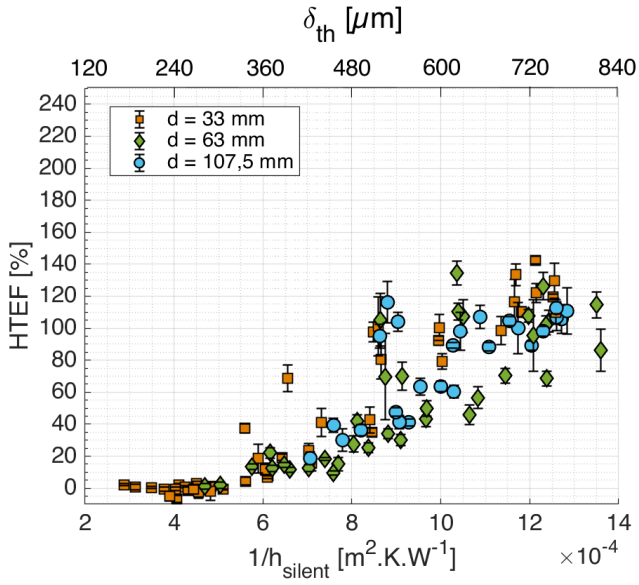

Figure 16 – Heat Transfer Enhancement Factor as a function of initial thermal resistance and corresponding estimated thermal boundary layer thickness for three channel widths (f_{us} = 2 MHz, P_{us} = 110 W).

0.6 W.K^{-1}.m^{-1}, it can be approximated as a thermal boundary layer of 360 µm, which corresponds to the order of magnitude of an acoustic cavitation bubble's radius of influence. Therefore, it could be suggested that heat transfer enhancement induced by acoustic cavitation depends on the quantity of bubbles that can be present within the thermal boundary layer. However, such assertion would require further investigations before it is confirmed.

In a similar way to the observations made for 25 kHz, HTEF with 2 MHz ultrasound follows an increasing trend as the thickness of thermal boundary layer increases. However, with 2 MHz ultrasound, unlike low frequency ultrasound, a minimum value of HTEF equal to 0% (meaning there is no enhancement) is measured below a certain thermal resistance of the initial thermal boundary layer, corresponding here to a value of $1/h_{silent}$ of $5 \cdot 10^{-4}$ $m^2.K.W^{-1}$.

On the other hand, HTEF values at block 1 tend to be higher than the results obtained with other blocks, and show larger standard deviations, which was also observed for 25 kHz ultrasound.

Nevertheless, with the exception of block 1, the HTEF values are less scattered, and the standard deviations are generally lower than those measured with 25 kHz ultrasound. Acoustic streaming appears to have a more reproducible effect on heat transfer enhancement than the acoustic cavitation produced at low frequency.

Thus, in the presence of 2 MHz ultrasound, heat transfer enhancement varies in a similar way to the enhancement induced by low frequency ultrasound, following a decreasing trend as the initial thickness of the thermal boundary layer in the silent regime decreases. However, the absence of acoustic cavitation with high-frequency ultrasound implies a greater decrease in HTEF. Consequently, below a certain thermal boundary layer thickness, and as demonstrated here, acoustic streaming produced by high frequency ultrasound no longer has an influence on heat transfer.

To summarize, the results presented here show that with a thicker thermal boundary layer, acoustic streaming or acoustic cavitation can more easily disturb the thermal boundary layer and thus enhance convective heat transfer. In this sense, ultrasound induces similar tendencies to other enhancement method for convective heat transfer, as it is usually easier to enhance convective heat transfer in laminar regime (i.e., in the presence of a thicker thermal boundary layer) than in turbulent regime (i.e., in the presence of a thinner thermal boundary layer).

4 Conclusions

In this work, heat transfer enhancement in forced convection using ultrasound has been analyzed, depending on ultrasonic frequency and the hydrodynamic conditions of the flow. For this purpose, an experimental set-up has been used, consisting of a rectangular channel through which thermally regulated water flows at a controlled flow rate. A heating plate equipped with thermocouples is positioned on one side, facing an ultrasonic transducer on the opposite side.

A hydrodynamic analysis has been performed to evaluate the ultrasonic effects as a function of the flow regime using Particle Image Velocimetry. A thermal approach has then been implemented to assess the convective heat transfer at different Reynolds numbers. The analysis was performed with low frequency ultrasound (25 kHz), which produces acoustic cavitation, and high frequency ultrasound (2 MHz), which produces acoustic streaming, emitted perpendicular to the water flow. Lastly, an analysis has been conducted on heat transfer enhancement as a function of the thermal boundary layer thickness and using different channel widths, resulting in different forced convection modes.

In the laminar regime, the presence of 25 kHz ultrasound, has demonstrated an increase of the averaged velocity gradient near the heating wall, meaning that the higher parietal shear stress is higher. The presence of low frequency ultrasound also results in the generation of turbulent kinetic energy within the flow, without pre-existing turbulence. This turbulent kinetic energy is mainly generated near the heating wall, facing the ultrasonic transducer. Consequently, in the laminar regime, 25 kHz ultrasound induces heat transfer enhancement. For Reynolds numbers in the range 900 to 2500, the HTEF at block 5 is between 110% and 120%. In the turbulent regime, the effect of 25 kHz ultrasound on the averaged velocity field becomes negligible. despite the fact that the acoustic cavitation intensifies the turbulent kinetic energy initially produced by the flow. However, the presence of acoustic cavitation at the wall allows heat transfer enhancement to be maintained in the turbulent regime. Indeed, with an increasing Reynolds number, the HTEF at the block 5 decreases until it reaches an asymptotic value around 50%, thus guaranteeing an enhancement of heat transfer regardless of the Reynolds number, within the range studied. By analyzing the heat transfer enhancement depending on the intial thermal boundary layer thickness, it appears that heat transfer enhancement induced by ultrasound decreases with decreasing thermal boundary layer thickness, regardless of the convection mode. However, 25 kHz ultrasound guarantees a minimum enhancement level of 40% for the entire heating plate, and across the whole range of water flow rates studied.

The influence of 2 MHz ultrasound on hydrodynamics and heat transfer varies greatly as a function of the flow regime. In the laminar regime, the presence of acoustic streaming, emitted perpendicular to the flow, results in a decrease in the velocity near the ultrasonic transducer, and an increase in the velocity near the heating wall. In addition, acoustic streaming leads to generation of turbulent kinetic energy within the flow. Thus, with the increase in velocity in the vicinity of the heating plate, the parietal shear stress increases. Consequently, these convective effects lead to enhancement of heat transfer in the laminar regime. In contrast, in the turbulent regime, acoustic streaming no longer has a significant effect on the mean velocity field, and the turbulent kinetic energy initially present in the flow is barely increased. Convective effects produced by acoustic streaming are thus considerably attenuated near the heating plate. Consequently, since acoustic streaming is the root cause of heat transfer enhancement with high frequency ultrasound, an increase in the Reynolds number results in a significant decrease in the HTEF, ultimately to 0% for Reynolds numbers over 7500. Furthermore, in a similar way to 25 kHz ultrasound, heat transfer enhancement produced by 2 MHz ultrasound is clearly related to the thickness of the thermal boundary layer. Indeed, reduction of the thermal boundary layer thickness results in a decrease of the HTEF, for all heating blocks and regardless of the convection mode, and no heat transfer enhancement is induced for a thin thermal boundary layer thickness.

References

[1] T. Alam and M.-H. Kim, "A comprehensive review on single phase heat transfer enhancement techniques in heat exchanger applications," *Renewable and Sustainable Energy Reviews*, vol. 81, pp. 813 – 839, 2018.

[2] Y. Yao, Y. Pan, and S. Liu, "Power ultrasound and its applications: A state-of-the-art review," *Ultrasonics Sonochemistry*, vol. 62, 2020. 104722.

[3] R. J. Wood, J. Lee, and M. J. Bussemaker, "A parametric review of sonochemistry: Control and augmentation of sonochemical activity in aqueous solutions," *Ultrasonics Sonochemistry*, vol. 38, p. 351–370, 2017.

[4] J. Sponer, "Dependence of the cavitation threshold on the ultrasonic frequency," *Czechoslovak Journal of Physics*, vol. 40, no. 10, pp. 1123–1132, 1990.

[5] M. Ashokkumar and F. Grieser, "Ultrasound assisted chemical processes," *Reviews in Chemical Engineering*, vol. 15, no. 1, pp. 41–83, 1999.

[6] S. Nomura, A. Yamamoto, and K. Murakami, "Ultrasonic heat transfer enhancement using a horn-type transducer," *Japanese Journal of Applied Physics*, vol. 41, pp. 3217–3222, 2002.

[7] S. Nomura, Y. Sasaki, and K. Murakami, "Flow pattern in a channel during application of ultrasonic vibration," *Japanese Journal of Applied Physics*, vol. 39, pp. 4987–4989, 2000.

[8] S. Nomura, K. Murakami, and M. Kawada, "Effects of turbulence by ultrasonic vibration on fluid flow in a rectangular channel," *Japanese Journal of Applied Physics*, vol. 41, pp. 6601–6605, 2002.

[9] S. Y. Lee and Y. D. Choi, "Turbulence generation by ultrasonically induced gaseous cavitation in the co2 saturated water flow," *KSME International Journal*, vol. 17, no. 8, pp. 1203–1210, 2003.

[10] O.Bulliard-Sauret, J. Berindei, S. Ferrouillat, L. Vignal, A. Memponteil, C. Poncet, J. Leveque, and N. Gondrexon, "Heat transfer intensification by low or high frequency ultrasound: Thermal and hydrodynamic phenomenological analysis," *Experimental Thermal and Fluid Science*, vol. 104, pp. 258–271, 2019.

[11] M. Barthès, G. Mazue, D. Bonnet, R. Viennet, J.-Y. Hihn, and Y. Bailly, "Characterization of the activity of ultrasound emitted in a perpendicular liquid flow using PIV and electrochemical mass transfer measurements," *Ultrasonics*, vol. 59, pp. 72–78, 2015.

[12] S. Hatanaka, H. Mitome, K. Yasui, and S. Hayashi, "Multibubble sonoluminescence enhancement by fluid flow," *Ultrasonics*, vol. 44, pp. e435–e438, 2006.

[13] O. Bulliard-Sauret, S. Ferrouilat, L. Vignal, A. Memponteil, and N. Gondrexon, "Heat transfer enhancement using 2 MHz ultrasound," *Ultrasonics sonochemistry*, vol. 39, pp. 262–271, 2017.

[14] H. Yukawa, T. Hoshino, and H. Saito, "Effect of ultrasonic vibration on free convection heat transfer from inclined plate in water," *Kagaku Kogaku Ronbunshu*, vol. 3, no. 1, pp. 229–234, 1975.

[15] D. Zhou, X. Hu, and D. Liu, "Local convective heat transfer from a horizontal tube in an acoustic cavitation field," *Journal of Thermal Sciences*, vol. 13, no. 4, pp. 338–343, 2004.

[16] S.-W. Chen, F.-C. Liu, H.-J. Lin, P.-S. Ruan, Y.-T. Su, Y.-C. Weng, J.-R. Wang, J.-D. Lee, and W.-K. Lin, "Experimental test and empirical correlation development for heat transfer enhancement under ultrasonic vibration," *Applied Thermal Engineering*, vol. 143, pp. 639–649, 2018.

[17] S. Nomura and M. Nakagawa, "Ultrasound enhancement of heat transfer on narrow surface," *Heat Transfer – Japanese research*, vol. 22, no. 6, pp. 546–558, 1993.

[18] S. Nomura, K. Murakami, Y. Aoyama, and J. Ochi, "Effect of changes in frequency of ultrasonic vibrations on heat transfer," *Heat Transfer–Asian research*, vol. 29, no. 5, pp. 358–372, 2000.

[19] M. Dehbani, M. Rahimi, and M. Abolhasani, "Cfd modeling of convection heat transfer using 1.7 MHz and 24 kHz ultrasonic waves: a comparative study," *Heat and Mass Transfer*, vol. 50, pp. 1319–1333, 2014.

[20] N. Gondrexon, Y. Rousselet, M. Legay, P. Boldo, S. L. Person, and A. Bontemps, "Intensification of heat transfer process – improvement of shell and tube heat exchanger performances by means of ultrasound," *Chemical Engineering and Processing : Process Intensification*, vol. 4, pp. 936–942, 2010.

[21] M. Legay, P. Boldo, N. Gondrexon, S. L. Person, and A. Bontemps, "Improvement of heat transfer by means of ultrasound – application to a double-tube heat exchanger," *Ultrasonics sonochemistry*, vol. 19, pp. 1194–1200, 2012.

[22] M. Setareh, M. Saffar-Avval, and A. Abdullah, "Experimental and numerical study on heat transfer enhancement using ultrasonic vibration in a double-pipe heat exchanger," *Applied Thermal Engineering*, vol. 159, 2019. 113867.

[23] N. Inworn and W. Chaiworapuek, "On the thermal characteristic of a heating flat surface under low frequency waves," *International Journal of Heat and Mass Transfer*, vol. 122, pp. 1153–1161, 2018.

[24] C. Poncet, S. Ferrouillat, L. Vignal, A. Memponteil, O. Bulliard-Sauret, and N. Gondrexon, "Enhancement of heat transfer in forced convection by using dual low-high frequency ultrasound," *Ultrasonics Sonochemistry*, vol. 71, 2021. 105351.

[25] T. Kimura, T. Sakamoto, J.-M. Leveque, H. Sohmiya, M. Fujita, S. Ikeda, and T. Ando, "Standardization of ultrasonic power for sonochemical reaction," *Ultrasonics Sonochemistry*, vol. 3, no. 3, pp. S157–S161, 1996.

[26] G. Mazue, R. Viennet, J.-Y. Hihn, D. Bonnet, M. Barthes, Y. Bailly, and I. Albaïna, "Influence of a perpendicular liquid flow on a cleaning process using 20 kHz ultrasound - characterization of the agitation at vicinity of the surface opposite to the transducer," *Canadian journal of chemical engineering*, vol. 93, pp. 201–205, 2015.

[27] J. J. O'Sullivan, C. J. Espinoza, O. Mihailova, and F. Alberini, "Characterisation of flow behaviour and velocity induced by ultrasound using particle image velocimetry (PIV): Effect of fluid rheology, acoustic intensity and transducer tip size," *Ultrasonics Sonochemistry*, vol. 48, pp. 218–230, 2018.

[28] LaVision, *Product Manual DaVis 8.3 Software*. Göttingen, 2015.

[29] G. Nellis and S. Klein, *Heat transfer*. Cambridge University Press, 2008.

[30] S. Kakaç, R. K. Shah, and W. Aung, *Handbook of single-phase Convective heat transfer*. John Wiley and Sons, 1987.

[31] D.-R. Lee and B. gook Loh, "Smart cooling technology utilizing acoustic streaming," *IEEE transactions on components and packaging technologies*, vol. 30, no. 4, pp. 691–699, 2007.

[32] M. Rahimi, M. Dehbani, and M. Abolhasani, "Experimental study on the effects of acoustic streaming of high frequency ultrasonic waves on convective heat transfer: Effects of transducer position and wave interference," *International Communications in Heat and Mass Transfer*, vol. 39, p. 720–725, 2012.

[33] M. Legay, S. L. Person, N. Gondrexon, P. Boldo, and A. Bontemps, "Performances of two heat exchangers assisted by ultrasound," *Applied Thermal Engineering*, vol. 37, pp. 60–66, 2012.

[34] Y. Yao, X. Zhang, and Y. Guo, "Experimental study on heat transfer enhancement of water shell and tube heat exchanger assisted by power ultrasonic," *International Refrigeration and Air Conditioning Conference*, 2010. Paper 1110.

[35] J. Cai, X. Huai, S. Liang, and X. Li, "Augmentation of natural convective heat transfer by acoustic cavitation," *Frontiers of Energy and Power Engineering in China*, vol. 4, no. 3, pp. 313–318, 2010.